Received: 29 July 2020 | Revised: 17 September 2020 | Accepted: 23 September 2020

DOI: 10.1002/ardp.202000277

Check for updates

FULL PAPER

DPhG ARCH PHARM Archiv der Pharmazie

Synthesis, antimicrobial evaluation, DNA gyrase inhibition, and in silico pharmacokinetic studies of novel quinoline derivatives

Mohamed H. El-Shershaby[1] | Kamal M. El-Gamal[1] | Ashraf H. Bayoumi[1] | Khaled El-Adl[2,3] | Hany E. A. Ahmed[1,4] | Hamada S. Abulkhair[1,5]

[1]Pharmaceutical Organic Chemistry Department, Faculty of Pharmacy, Al-Azhar University, Cairo, Egypt

[2]Pharmaceutical Medicinal Chemistry & Drug Design Department, Faculty of Pharmacy, Al-Azhar University, Cairo, Egypt

[3]Department of Pharmaceutical Chemistry, Faculty of Pharmacy, Heliopolis University for Sustainable Development, Cairo, Egypt

[4]Pharmacognosy and Pharmaceutical Chemistry Department, Taibah University, Al-Madinah Al-Munawarah, Saudi Arabia

[5]Pharmaceutical Chemistry Department, Faculty of Pharmacy, Horus University, New Damietta, Egypt

Correspondence
Hamada S. Abulkhair, Pharmaceutical Organic Chemistry Department, Faculty of Pharmacy, Al-Azhar University, Nasr City, Cairo 11884, Egypt.
Email: hamadaorganic@azhar.edu.eg

Abstract

Herein, we report the synthesis and in vitro antimicrobial evaluation of novel quinoline derivatives as DNA gyrase inhibitors. The preliminary antimicrobial activity was assessed against a panel of pathogenic microbes including Gram-positive bacteria (*Streptococcus pneumoniae* and *Bacillus subtilis*), Gram-negative bacteria (*Pseudomonas aeruginosa* and *Escherichia coli*), and fungal strains (*Aspergillus fumigatus*, *Syncephalastrum racemosum*, *Geotrichum candidum*, and *Candida albicans*). Compounds that revealed the best activity were subjected to further biological studies to determine their minimum inhibitory concentrations (MICs) against the selected pathogens as well as their in vitro activity against the *E. coli* DNA gyrase, to realize whether their antimicrobial action is mediated via inhibition of this enzyme. Four of the new derivatives (**14**, **17**, **20**, and **23**) demonstrated a relatively potent antimicrobial activity with MIC values in the range of 0.66–5.29 μg/ml. Among them, compound **14** exhibited a particularly potent broad-spectrum antimicrobial activity against most of the tested strains of bacteria and fungi, with MIC values in the range of 0.66–3.98 μg/ml. A subsequent in vitro investigation against the bacterial DNA gyrase target enzyme revealed a significant potent inhibitory activity of quinoline derivative **14**, which can be observed from its IC_{50} value (3.39 μM). Also, a molecular docking study of the most active compounds was carried out to explore the binding affinity of the new ligands toward the active site of DNA gyrase enzyme as a proposed target of their activity. Furthermore, the ADMET profiles of the most highly effective derivatives were analyzed to evaluate their potentials to be developed as good drug candidates.

KEYWORDS

antimicrobial, DNA gyrase, molecular docking, quinoline, synthesis

1 | INTRODUCTION

A wide-ranging panel of infectious diseases including bacterial and fungal infections is becoming resistant to commonly prescribed drugs.[1] This resistance is the main obstacle to the management of global infectious diseases. The World Health Organization has recognized this antimicrobial resistance and the dwindling number of current potent antimicrobial drugs to be alarming threats to human health.[2] Also, problems of vancomycin-resistant and methicillin-resistant *Staphylococcus*

 © 2020 Deutsche Pharmazeutische Gesellschaft

aureus (VRSA and MRSA, respectively) and fluconazole-resistant *Candida* have reached a disturbing level worldwide.[3] Consequently, it is essential to develop new antimicrobial agents with improved potency.

DNA gyrase is a topoisomerase II that is vital in the DNA transcription and replication processes in eukaryotes.[4] Quinolone antimicrobials are the oldest, and still the only, existing class of agents clinically used to inhibit bacterial DNA synthesis.[5] Nalidixic acid (**1**) is a quinolone that forms the basis of the development of the fluoroquinolone class of compounds. Fluoroquinolones and their analogous naphthyridine antibiotics (Figure 1) work as DNA gyrase poisons, as they could stabilize the covalent gyrase–DNA complex,[5] thereby leading to protein-stabilized DNA breaks and eventually cell death. Nalidixic acid was first introduced into the market in the late 60s of the past century for the treatment of urinary tract infections.[6] Subsequent novel generations of fluoroquinolones with improved efficacy were afterward developed, namely norfloxacin (**2**), ciprofloxacin (Cipro, **3**), levofloxacin (Levaquin, **4**), moxifloxacin (Avelox, **5**), gemifloxacin (Factive, **6**), and delafloxacin (Baxdela, **7**). Over the last two decades, there were several reports on novel quinoline derivatives as potential antimicrobial agents that target DNA gyrase.[7,8] Currently, fluoroquinolones are being utilized in the management of serious microbial infections such as bacterial pneumonia. However, bacterial resistance to such antimicrobials with no novel medications in the antimicrobials pipeline has driven intensive research in this area.

However, pathogenic fungi are one of the most harmful parasitic organisms and can cause serious health problems. Fungal infections also produce various toxins that can seriously compromise food safety.[9] Over the last few decades, the use of a huge number of antifungal agents has resulted in resistance to eradicate fungi, thus leading to a decrease in the efficacy of traditional fungicides. Consequently, it is also essential to develop novel effective fungicides to control these fungal diseases. Quinoline is a vital pharmacophore ring system present in a number of antifungal agents.[8,10] Quinoline derivatives possess diverse pharmacological activities, particularly antibacterial,[7,8] antifungal,[8,11–13] and antimalarial.[14,15]

1.1 | Rationale and aim of the work

On the basis of the aforementioned facts, inspired by the versatility of the quinoline moiety mentioned above, and as a continuation of our recent studies,[7,16,17] to identify new antimicrobial agents, the synthesis of three novel series of 6-methylquinoline-3-carbonitrile derivatives was carried out to obtain new molecules with higher potency. The design of new compounds depended on modifying structural aspects of the previously reported fluoroquinolones to evaluate their activities against pathogenic bacterial and fungal strains. The fluorine atom was replaced by the methyl group, the carbonitrile group was attached to C-3, and different substitution patterns were introduced into C-2 of the quinoline scaffold to investigate the effect of such substitution pattern on the antimicrobial activity of the designed compounds. All the synthesized compounds were evaluated for their in vitro antimicrobial activity against a panel of pathogenic microbes including two Gram-positive bacteria (*Streptococcus pneumoniae* and *Bacillus subtilis*), two Gram-negative bacteria (*Pseudomonas aeruginosa* and *Escherichia coli*), and four fungal strains (*Aspergillus fumigatus*, *Syncephalastrum racemosum*, *Geotrichum candidum*, and *Candida albicans*). In addition, the structure–activity relationship of the synthesized compounds was discussed. Also, a molecular docking study of the most active compounds was carried out to predict the binding affinity toward the active site of DNA gyrase enzyme as a proposed target of their activity. Furthermore, absorption, distribution, metabolism, excretion, and toxicity (ADMET) profiles of the highest effective derivatives were examined to evaluate the potentials of new compounds to be developed as good drug candidates.

2 | RESULTS AND DISCUSSION

2.1 | Chemistry

Synthetic approaches adopted for the synthesis of the starting 2-mercapto-6-methylquinoline-3-carbonitrile and final target compounds are illustrated in Schemes 1 and 2. The starting material, 2-mercapto-6-methylquinoline-3-carbonitrile (**11**), was prepared by

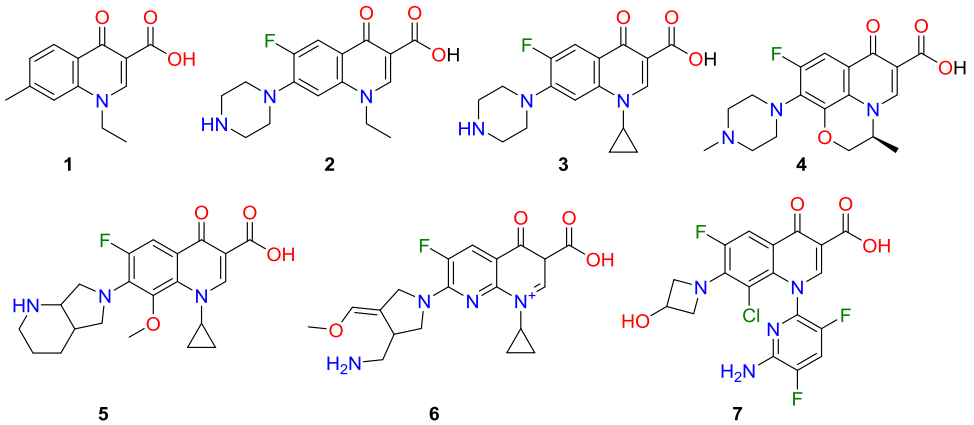

FIGURE 1 Fluoroquinolones and their analogous naphthyridine antibiotics

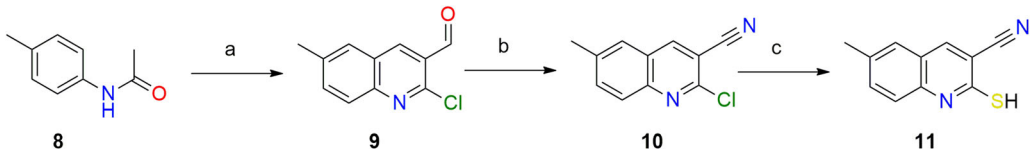

Reagents and Conditions

a) $POCl_3$/DMF, 0 °C, 8 h, 72%; b) $NH_2OH.HCl$, 70-110 °C, 2 h, 80%; c) $(NH_2)_2CS$, 120 °C, 8 h, 80%

SCHEME 1 The synthetic protocol of the starting quinoline

the Vilsmeier–Haack reaction[18] of *p*-methylacetanilide with dimethylformamide (DMF) and phosphorus oxychloride, followed by treatment of the produced quinoline-3-carbaldehyde derivative with hydroxylamine hydrochloride to give 2-chloro-6-methylquinoline-3-carbonitrile (**10**). Treating the latter with thiourea gave 6-methyl-2-mercaptoquinoline-3-carbonitrile,[19] which was used as a starting material in the synthesis of final compounds. In the present work, the Vilsmeier–Haack method was selected to prepare the first intermediate, **9**, due to the availability of starting materials and accessible reaction conditions. Briefly, DMF and $POCl_3$ were allowed to react at 0°C for 2 hr, and then *p*-methylacetanilide was added to the reaction mixture. The overall reactant ratio was found to be a critical issue to obtain the desired product in a good yield. Different ratios have been tried and the optimum one was 1:3:12 (**8**/DMF/$POCl_3$). Compound **10** was obtained in a high yield, 80%, using a Bell and Ackerman modified protocol, where compound **9** was treated with hydroxylamine hydrochloride at 70°C for 2 hr. Then, the in situ formed oxime was directly heated up to 110°C to lose a molecule of water and give the desired quinoline-3-carbonitrile product. The starting quinoline derivative **11** was prepared following the reported procedure in an 80% yield. Briefly, compound **10** was allowed to react with thiourea, followed by treating the reaction mixture with sodium hydroxide. The reaction mechanism involves the formation of an isothiuronium salt, which is converted to the mercapto-containing compound upon the addition of sodium hydroxide. Both the melting point and infrared (IR) spectrum confirmed the structure of the compound, where a characteristic SH broad absorption band was observed at 2,624 cm^{-1}.

As depicted in Scheme 2, our convergent synthesis approach to the final compounds started with the preparation of *N*-aryl-2-chloroacetamides and *N*-aryl-3-chloropropionamides by the reaction of substituted anilines with 2-chloroacetyl chloride or 3-chloropropionyl chloride in the presence of triethylamine.[20,21,22] Similarly, α-chloroacetate and α-chloropropionate esters were obtained by the action of α-chloroacetyl chloride or α-chloropropionyl chloride against the appropriate alcohol.[23,24] Final target quinolines of the current work were achieved by the electrophilic substitution of starting 2-mercapto-6-methylquinoline-3-carbonitrile with different electrophiles including the

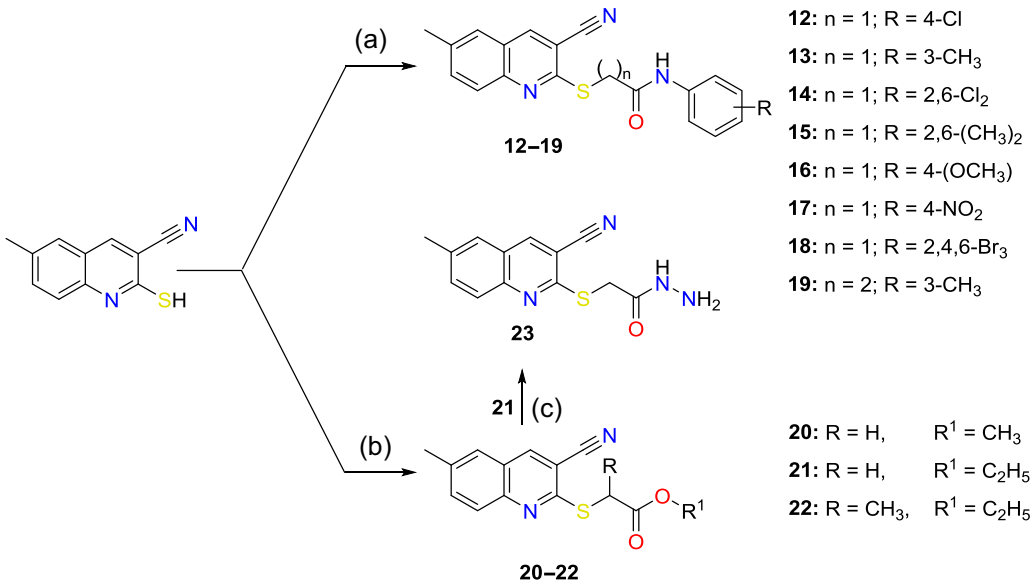

12: n = 1; R = 4-Cl
13: n = 1; R = 3-CH_3
14: n = 1; R = 2,6-Cl_2
15: n = 1; R = 2,6-$(CH_3)_2$
16: n = 1; R = 4-(OCH_3)
17: n = 1; R = 4-NO_2
18: n = 1; R = 2,4,6-Br_3
19: n = 2; R = 3-CH_3

20: R = H, R^1 = CH_3
21: R = H, R^1 = C_2H_5
22: R = CH_3, R^1 = C_2H_5

Reagents and Conditions

a) $Cl(CH_2)_2CONHAr/K_2CO_3$/DMF, 120 °C, 7 hr, 70–85%;
b) $ClCH(R)COOR^1/K_2CO_3$/DMF, 120 °C, 9 hr, 70–85%;
c) $NH_2NH_2.H_2O/C_2H_5OH$, 90 °C, 3 hr, 92%

SCHEME 2 The synthetic route of the new quinoline derivatives

above-prepared 2-chloro-*N*-arylacetamide, 3-chloro-*N*-arylpropanamide, α-chloroactate, and α-chloropropionate ester derivatives in the presence of potassium carbonate to neutralize the effect of HCl side product.[25,26]

The progress of the chemical reactions was validated by thin-layer chromatography (TLC) methodology and the final products were purified by the column chromatography method. Structures and purities of new derivatives were confirmed on the basis of their IR, liquid chromatography–mass spectrometry, ^{1}H nuclear magnetic resonance (NMR), and ^{13}C NMR spectral data. In all cases, the characteristic thiol stretching band disappeared and typical amide or ester carbonyl stretching bands were observed between 1,660 and 1,725 cm^{-1}, as revealed by all IR spectra. Collectively, these observations confirm tethering of the acetanilide moiety with the quinoline nucleus of compounds **12**–**19** via S-linkage. The NH group revealed a D_2O-exchangeable singlet, equivalent to one proton, around 10.40 ppm. The ^{1}H NMR spectra of compounds **12**–**19** showed, in addition to quinoline aromatic protons, aromatic signals equivalent to aromatic acetanilide protons and one D_2O-exchangeable singlet signal equivalent to one proton, around 10.30 ppm due to NH. The aliphatic S–CH_2 protons appeared as a singlet signal at about 4.20 ppm, a singlet signal equivalent to three protons at 2.50 ppm due to quinoline-CH_3. Also, IR spectra of all compounds showed stretching bands in the range of 3,419 and 3,460 cm^{-1}, representing the secondary amide NH functionality. In addition, typical amidic carbonyl stretching bands between 1,665 and 1,681 cm^{-1} were observed. The ^{13}C NMR spectra of acetamide derivatives **12**–**19** are characterized by the presence of a minimum of two peaks in the aliphatic region at ~34 ppm due to SCH_2 and ~19 ppm due to CH_3. The most predominant features in the IR spectra of the isolated ester derivatives **20**–**22** were the disappearance of the thiol-characteristic band at 2,624 cm^{-1}, which reflects S-substitution, and the appearance of a distinctive carbonyl ester stretching band around 1,730 cm^{-1}. In addition, the protons of added alkyl ester moieties were revealed in the ^{1}H NMR spectra between 4.60 and 1.30 ppm. The ethyl acetate moiety of compound **21** showed a singlet signal equivalent to two protons at 3.30 ppm due to S–CH_2, a quartet signal of two protons at 4.30 ppm, and a triplet of three protons at 1.30 ppm, with the same coupling constant, due to ethoxy group. The ^{1}H NMR spectrum of the propionate analog **22** showed two distinctive signals, that is, a doublet equivalent to the methyl group at 1.15 ppm and a quartet signal at 4.10 ppm, equivalent to a methine proton, with the same *J* value. Both signals confirm the presence of ethyl propionate moiety substituted at carbonyl carbon. The ^{1}H NMR spectra of hydrazide **23** is characterized by the presence of a singlet signal at 8.86 ppm, which is corresponding to one proton of NH. The presence of a signal at 4.30 ppm indicates two protons of NH_2. Besides, the presence of a singlet signal at 4.0 ppm indicates two protons of S–CH_2. Mass spectra of all the new structures are characterized by the presence of distinctive molecular ion peaks at the expected *m/z* value. All the newly synthesized triazoles gave elemental analysis data consistent with that calculated for assigned structures.

2.2 | Evaluation of biological activity

2.2.1 | Antibacterial activity

All the newly synthesized compounds were evaluated for their in vitro antibacterial activities against the four bacterial pathogens:

TABLE 1 Antibacterial activity of the new compounds against Gram-positive and Gram-negative pathogens

Compound no.	Inhibition zone (mm)[a]			
	Streptococcus pneumoniae	*Bacillus subtilis*	*Pseudomonas aeruginosa*	*Escherichia coli*
12	18.1 ± 0.72	20.2.1 ± 0.58	NA	16.6 ± 0.72
13	17.4 ± .58	19.1 ± 0.63	NA	15.2 ± 0.58
14	19.3 ± 0.58	20.8 ± 0.67	NA	19.2 ± 0.63
15	NA	NA	NA	NA
16	17.1 ± 0.44	17.9 ± 0.63	NA	16.7 ± 2.1
17	19.3 ± 0.58	21.2 ± 0.72	NA	18.3 ± 0.63
18	NA	NA	NA	NA
19	13.6 ± 1.2	15.2 ± 1.5	NA	12.4 ± .58
20	20.3 ± 0.58	21.4 ± 1.2	NA	20.3 ± 0.58
21	15.7 ± 2.1	16.1 ± 0.58	NA	15.2 ± 0.63
22	18.3 ± .63	20.4 ± 0.63	NA	17.5 ± 2.1
23	20.7 ± 0.72	21.8 ± 0.63	NA	20.9 ± 0.58
Ampicillin	23.8 ± 0.2	32.4 ± 0.58	NT	NT
Gentamicin	NT	NT	17.3 ± 0.63	21.3 ± 0.58

Abbreviations: NA, no activity; NT, not tested.

[a]Mean zone of inhibition in millimeters ± standard deviation for at least three experiments.

S. pneumoniae and *B. subtilis* as examples of Gram-positive bacteria; *P. aeruginosa* and *E. coli* as examples of Gram-negative bacteria. Results of the antibacterial activity of new compounds are presented in Table 1. Agar diffusion method[27,28] was used for the preliminary evaluation of antibacterial activity and results were listed as the average diameter of inhibition zones (IZs) of bacterial growth around the discs in millimeters. Ampicillin and gentamycin (1 mg/ml) were used as standard references for Gram-positive and Gram-negative bacteria, respectively.

2.2.2 | Antifungal activity

The synthesized compounds were tested in vitro for their antifungal activity against four human pathogenic strains: *A. fumigatus*, *S. racemosum*, *G. candidum*, and *C. albicans*. The agar diffusion method[27,28] was also used for the evaluation of the initial screening of antifungal activities. Amphotericin B (1 mg/ml) was used as a positive control. Results for each test compound were recorded as the average diameter of IZs, in millimeters, of fungal growth around the discs. IZ diameters, attributed to the tested original concentration (5 mg/ml) as a preliminary test, are shown in Table 2.

2.2.3 | Structure–activity relationship study

From the above-mentioned data, the following observation can be made: The mean values of the inhibitory zone diameter obtained for the new compounds suggest that all the new derivatives possess a significant antimicrobial activity against most of the tested bacterial and fungal pathogens. Results of antimicrobial screening showed that most of the studied compounds displayed variable growth inhibitory effects on the tested Gram-positive and Gram-negative bacterial strains and fungal strains. In general, most of the tested quinolines revealed a higher activity against the Gram-positive strains than Gram-negative strains. It was also observed that there is no significant variation between the antimicrobial activity of amide derivatives **12**–**19** and both of ester derivatives **20**–**22** and hydrazide **23**. As expected, a clear difference in the activity is noted between derivatives within the same series, pointing to the strengthening and fading effects of substitution at C-2 of the quinoline scaffold. The diameter of IZs of the antifungal activity revealed almost the same trend as the antibacterial activity. Concerning the effect of substitution at the terminal phenyl ring in amide derivatives **12**–**19**, it is evident that the change of such a substituent may have a remarkable effect on the antimicrobial activity, which may be improved or decreased, depending on the electronic nature of such a substituent. The type of the substitutions on the terminal phenyl ring is important. Except for compound **18**, amide derivatives with electron-withdrawing substituents (**12**, **14**, and **17**) showed better activity than other derivatives with electron-donating substituents. The diminished activity of **18** may be attributed to the presence of three bulky bromine atoms, which may interfere with the binding of such compounds with the receptor site. Elongation of the linker moiety of these amides, as in compound **19**, revealed a negative impact on the antimicrobial activity. Regarding esters **20**–**22**, it was concluded that the acetate derivatives **20** and **21** showed much better activity than that of the propionate derivative **22**. The hydrazide derivative **23**

TABLE 2 Antifungal activity of the new compounds

Compound no.	Inhibition zone (mm)[a]			
	Aspergillus fumigatus	*Syncephalastrum racemosum*	*Geotrichum candidum*	*Candida albicans*
12	19.3 ± 2.1	17.2 ± 0.25	19.9 ± 1.5	NA
13	17.3 ± 1.2	16.2 ± 0.44	18.3 ± 2.1	NA
14	20.1 ± 1.2	18.3 ± 0.58	20.1 ± 2.1	NA
15	NA	NA	NA	NA
16	NA	NA	NA	NA
17	18.3 ± 1.2	19.3 ± 0.58	20.4 ± 2.1	NA
18	NA	NA	NA	NA
19	NA	NA	NA	NA
20	19.3 ± 0.63	19.9 ± 2.1	20.6 ± 0.58	NA
21	NA	NA	NA	NA
22	17.3 ± 2.1	16.4 ± 0.58	19.1 ± 1.5	NA
23	19.5 ± 1.2	20.1 ± 0.63	21.3 ± 2.1	NA
Amphotericin B	23.7 ± 0.63	19.7 ± 0.72	28.7 ± 0.58	25.4 ± 0.63

Abbreviation: NA, no activity.
[a]Mean zone of inhibition in millimeters ± standard deviation for at least three experiments.

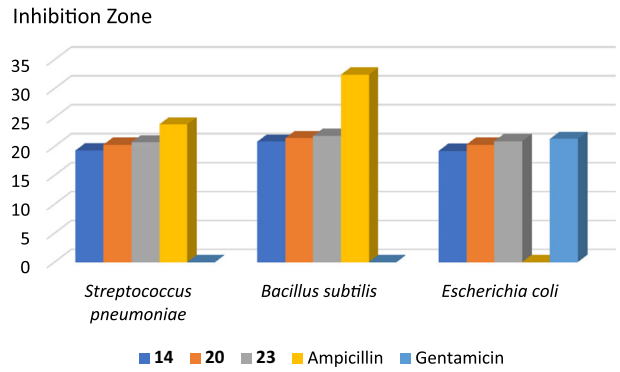

FIGURE 2 The comparison between the inhibition zones of compounds **14**, **20**, and **23**, and standard drugs against three tested Gram-positive and Gram-negative bacterial strains

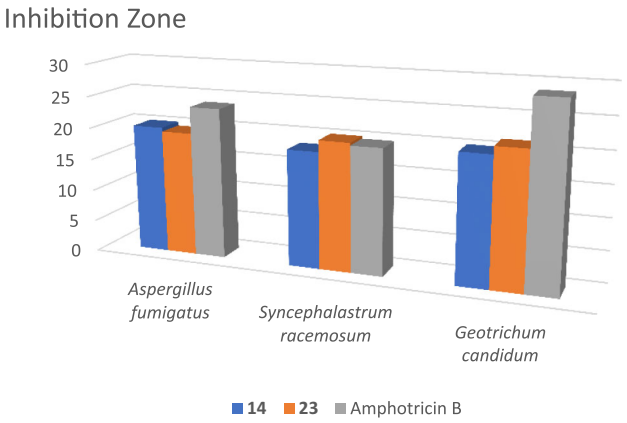

FIGURE 3 The comparison between the inhibition zones of compounds **14** and **23** and standard drug against three tested fungal strains

showed promising activities against all the selected bacterial and fungal strains, except *P. aeruginosa* and *C. albicans*.

In particular, the antibacterial activity of the synthesized compounds revealed that the highest activity against *S. pneumoniae* was obtained with compounds **20** and **23**, which gave very promising results with activity ≥85% in comparison to the standard drugs. Also, the same two compounds showed the best activity against *B. subtilis* and the Gram-negative strain *E. coli*, which gave 66% and 96% efficacy, respectively, relative to those of ampicillin and gentamicin. No activity was observed against *P. aeruginosa* with any of the tested compounds.

Regarding the antifungal activity, the highest potent compound against *A. fumigatus* was **14** with 84.8% efficacy in comparison to the standard drug. The best activities against *S. racemosum* and *G. candidum* were observed in the case of compound **23**, with 95.12% and 74.2% efficacy, respectively, in comparison to amphotericin B. No activity was observed against *Candida albicans* with any of the tested compounds. A summary of the structure–activity relationship of the most active derivatives, compared with standard antimicrobial agents, is presented in Figures 2 and 3.

2.2.4 | Minimum inhibitory concentration (MIC) and in vitro enzyme assay

Compounds that revealed the highest potent activity in the preliminary antimicrobial evaluation (**14**, **17**, **20**, and **23**) were subjected to further biological studies to determine their MICs[29] against the selected bacterial and fungal pathogens as well as their in vitro activity against the *E. coli* DNA gyrase. The in vitro capability of selected compounds to inhibit DNA gyrase enzyme was evaluated using the DNA gyrase supercoiling assay[30] to realize whether their effect is mediated via inhibition of this enzyme. Novobiocin was used as a positive control. The obtained MIC values, together with the IC_{50} values, of these compounds as DNA gyrase inhibitors and reference drugs are presented in Table 3. The tabulated results revealed that the amide derivatives **14** and **17** showed low MIC values as compared with the ester and hydrazide derivatives **20** and **23**. In particular, the compound with two halogen substituents (**14**) was the highest potent compound with MIC values of 0.98, 0.74, 3.98, 0.79,

TABLE 3 Minimum inhibitory concentrations (MIC in μg/ml) and DNA gyrase activity (IC_{50} in μM) of new compounds

	Minimum inhibitory concentrations (MIC in μg/ml)								
	Gram-positive bacteria		Gram-negative bacteria		Fungi				DNA gyrase activity (IC_{50} in μM)
Compound no.	*Streptococcus pneumoniae*	*Bacillus subtilis*	*Pseudomonas aeruginosa*	*Escherichia coli*	*Aspergillus fumigatus*	*Syncephalastrum racemosum*	*Geotrichum candidum*	*Candida albicans*	
14	0.98	0.74	NT	3.98	0.79	3.80	0.66	NT	3.39 ± 0.25
17	1.15	0.98	NT	4.21	1.35	3.93	0.98	NT	7.10 ± 1.50
20	2.15	1.82	NT	5.49	1.49	4.65	1.04	NT	26.50 ± 1.32
23	1.95	1.95	NT	4.49	1.28	4.07	0.98	NT	18.52 ± 1.05
Ampicillin	0.96	0.47	NT	NT	NT	NT	NT	NT	NT
Gentamicin	NT	NT	15.38	3.70	NT	NT	NT	NT	NT
Amphotericin B	NT	NT	NT	NT	0.92	3.96	0.51	0.51	NT
Novobiocin	NT	NT	NT	NT	NT	NT	NT	NT	1.84 ± 0.11

Abbreviation: NT, not tested.

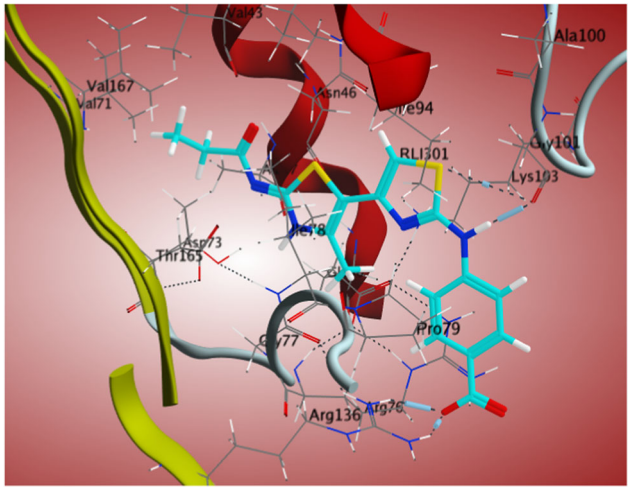

FIGURE 4 Three-dimensional interactions of RLI with the active site of DNA gyrase

3.80, and 0.66 μg/ml against *S. pneumoniae*, *B. subtilis*, *E. coli*, *A. fumigatus*, *S. racemosum*, and *G. candidum*, respectively, compared with 0.96, 0.47, 3.70, 0.92, 3.96, and 0.51 μg/ml of reference drugs. Also, the same compound revealed the best activity as a DNA gyrase inhibitor with an IC_{50} value of 3.39 μM as compared with 1.84 μM of novobiocin.

2.3 | Molecular docking study

To rationalize the mechanism of action of the four most active compounds, a molecular docking study was conducted to give guidance concerning their molecular binding modes inside the pocket of DNA gyrase enzyme. The in silico docking study was performed using Molecular Operating Environment (MOE) software, utilizing the flexible docking protocol implemented in the MOE software, and using the 4DUH complex retrieved from Protein Data Bank. The latter complex was prepared by the removal of solvent molecules and the internal ligand, followed by protonation of protein. Initially, a flexible docking of the original ligand (RLI) was carried out to validate the reliability of this enzyme model. Next, one of the four most active compounds was added for computational analysis. At the end of the molecular docking procedure, docking poses were scored and selected, depending on the calculated energy of binding. The binding mode of the original co-crystallized ligand, RLI[31] with the pocket of DNA gyrase enzyme, exhibited a binding energy of −13.85 kcal/mol. There are two main interactions between RLI and the binding site of the receptor (Figure 4): (a) two hydrogen-bonding interactions between the terminal carboxylate group of RLI and Arg76 and Arg136 residues; (b) two hydrogen-bonding interactions between the NH and S atom of the thiazole ring of RLI and the Gly101 residue. Free energies of binding, hydrophobic interaction, and hydrogen bonding interactions of selected compounds and that of the original ligand are presented in Table 4.

The behavior of the new compounds in the pocket of DNA gyrase is summarized in Figure 5, which is almost similar to the RLI drug. The binding mode of compound **14** exhibited an affinity value of −13.59 kcal/mol, which is much better than that of the internal ligand. Adhering to almost the same interaction pattern of RLI with the binding site of DNA gyrase, the carbonyl oxygen of **14** formed a hydrogen bond with the Arg136 residue. The sulfur atom formed one more hydrogen bond with the Glu50 residue. An additional hydrophobic interaction is formed between the quinoline ring scaffold and the Arg136 residue (Figure 5). These three desirable interactions of compound **14** might explain the good activity of such derivative as an antimicrobial agent. Independently, compound **17** revealed an affinity value of −10.49 kcal/mol and exhibited a different virtual binding

TABLE 4 In silico docking results of the most active compounds with the binding site of DNA gyrase

Compound no.	ΔG (kcal/mol)	Hydrogen bonding interactions		Hydrophobic interaction
		Distance (Å)	Residue	
14	−13.59	3.16 3.12 3.28	Arg136 Glu50 Gly101	Arg136
17	−10.49	3.68 2.61	Asn46 Lys103	–
20	−12.68	3.35 2.94	Asp73 Gly77	Lys103
23	−11.10	3.01 bidirectional 3.40 2.94	Asp73 Asp73 Gly77	Lys103
RLI	−12.23	3.06 3.15 3.63 bidirectional 2.81	Arg76 Arg136 Gly101 Gly101	–

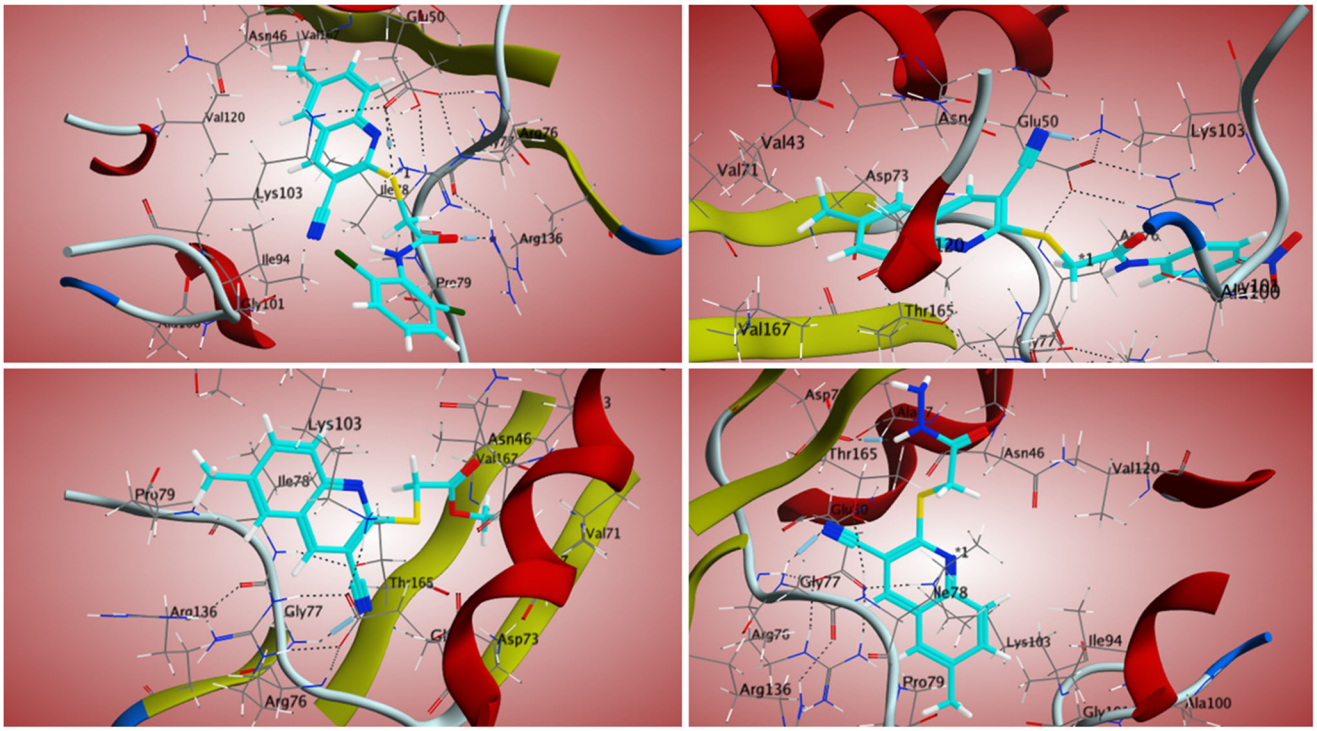

FIGURE 5 Three-dimensional interactions of compounds **14** (upper left panel), **17** (upper right panel), **20** (lower left panel), and **23** (lower right panel) with the active site of DNA gyrase enzyme

mode with the DNA gyrase enzyme. The nitrile nitrogen formed a hydrogen bond with Lys103 residue, whereas the sulfur atom formed another hydrogen bond with the Asn46 residue. The ester derivative **20** also exhibited a different virtual binding mode with that of **14**. The ester derivative **20** revealed an affinity value of −10.98 kcal/mol and showed three different interaction patterns with the binding site of DNA gyrase receptor. These interactions involve two hydrogen bonds between the sulfur atom and nitrile nitrogen in the target compounds with Asp73 and Gly77 residues, respectively. The third interaction is the form of arene–H hydrophobic interaction between the benzene of quinoline ring scaffold and the Lys103 residue. The obtained docking result for the hydrazide derivative **23** is virtually the same as that of compound **20**. With −11.10 kcal/mol free energy of binding, the binding mode of **23** involves two hydrogen bonds between the sulfur atom and nitrile nitrogen in the target compounds with Asp73 and Gly77 residues, respectively. A bidirectional hydrogen bond is also formed between the NH fragment of **23** and the Asp73 residue. The last interaction is similar to that of **20**, an arene–H hydrophobic interaction between the benzene of quinoline ring scaffold and the Lys103 residue.

2.4 | Pharmacokinetic study

In the present study, an in silico computational analysis of compounds with a promising antimicrobial activity was conducted to determine their surface areas and other physicochemical properties according to directions of the Lipinski's rule of five.[32] Lipinski proposed that the absorption of an orally administered compound is more likely to be good enough if the molecule obeys at least three rules of the following: (a) molecular weight <500; (b) H-bond donors (OH, NH, and SH) ≤ 5; (c) H-bond acceptors (N, O, and S atoms) ≤ 10; (d) log*P* < 5. The bioavailability of molecules that violate more than one of these rules is expected to be not good. Whereas the reference compound drugs gentamicin and amphotericin B violated two or more of Lipinski's rules, all the highest active derivatives in this study satisfied all the Lipinski's rules, except compound **14**, which only violated log*P*. All derivatives own a limited number of hydrogen bond acceptors (between 4 and 6) and only two or less hydrogen bond donor groups. These numbers of H-bond acceptors and donors in the new compounds agree satisfactorily with Lipinski's rules. In addition, ADMET profiles of the new quinoline derivatives were preliminary evaluated to determine their possibility to be developed as good oral drug candidates. The pharmacokinetic profile of a compound detects how it would be absorbed, distributed, metabolized, and excreted (ADME). Although the ideal binding of a drug to the protein target is critical, making sure that it will arrive at this therapeutic target in a relatively adequate concentration is also essential to produce the biological effect. ADMET profiles have been predicted using the pkCSM descriptors algorithm protocol.[33] Two main structural aspects correlate properly with pharmacokinetic properties, the 2D polar surface area (PSA_2D) and the lipophilicity levels (log*P*). The absorption of a drug depends on several factors including intestinal absorption, membrane permeability, skin permeability, and P-glycoprotein substrate or inhibitor. Drug distribution depends on the

TABLE 5 ADMET profile of the four most active compounds and reference drugs

Parameter	14	17	20	23	Ampicillin	Gentamicin	Amphotericin B
Molecular properties							
Molecular weight	402.306	378.413	272.329	272.333	349.412	477.603	924.091
Log*P*	5.4525	4.0539	2.68	1.4969	0.3181	−3.3275	0.7117
Rotatable bonds	4	5	3	3	4	7	3
H-bond acceptors	4	6	5	5	5	12	17
H-bond donors	1	1	0	2	3	8	12
Surface area	164.683	158.730	114.948	114.330	143.121	194.977	380.536
Absorption							
Water solubility	−5.713	−4.922	−3.418	−2.638	−2.396	−2.56	−2.937
Caco2 permeability	0.618	0.899	1.062	−0.105	0.395	−0.164	−0.597
Intestinal abs. (human)	91.751	95.038	97.334	84.168	43.034	13.46	0
Skin permeability	−2.822	−2.769	−2.642	−3.069	−2.735	−2.735	−2.735
P-glycoprotein substrate	Yes	Yes	No	Yes	No	Yes	Yes
P-glycoprotein I inhibitor	Yes	Yes	No	No	No	No	No
P-glycoprotein II inhibitor	Yes	Yes	No	No	No	No	No
Distribution							
VDss (human)	0.09	−0.076	−0.175	−0.178	−1.23	−0.967	−0.37
Fraction unbound (human)	0.027	0.022	0.196	0.247	0.752	0.94	0.541
BBB permeability	0.072	−0.648	−0.26	−0.474	−0.767	−1.593	−2.058
CNS permeability	−1.554	−1.996	−2.853	−2.939	−3.166	−5.49	−3.718
Metabolism							
CYP2D6 substrate	No	No	No	No	No	No	No
CYP3A4 substrate	Yes	Yes	No	Yes	No	No	No
CYP1A2 inhibitor	Yes	Yes	Yes	Yes	No	No	No
CYP2C19 inhibitor	Yes	Yes	Yes	No	No	No	No
CYP2C9 inhibitor	Yes	Yes	No	No	No	No	No
CYP2D6 inhibitor	No	No	No	No	No	No	No
CYP3A4 inhibitor	Yes	Yes	No	No	No	No	No
Excretion							
Total clearance	0.307	0.139	0.427	0.082	0.337	0.722	−1.495
Renal OCT2 substrate	Yes	No	No	No	No	No	No
Toxicity							
Ames toxicity	Yes	Yes	Yes	Yes	No	No	No
Max. tolerated dose (human)	0.281	0.038	0.513	0.338	0.952	0.694	0.292
hERG I inhibitor	No	No	No	No	No	No	No
hERG II inhibitor	Yes	No	No	No	No	No	No
Oral rat acute toxicity (LD_{50})	2.424	2.721	2.336	2.582	1.637	2.016	2.518
Oral rat chronic toxicity (LOAEL)	0.711	1.346	0.743	1.447	2.398	3.506	2.049
Hepatotoxicity	No	Yes	Yes	Yes	Yes	No	No
Skin sensitization	No	No	No	No	No	No	No
Tetrahymena pyriformis toxicity	1.515	0.857	1.073	0.584	0.285	0.285	0.285
Minnow toxicity	−2.85	−2.108	−0.327	2.279	4.232	5.959	11.261

Abbreviations: BBB, blood–brain barrier; CNS, central nervous system; VDss, volume of distribution.

volume of distribution (VDss), the blood–brain barrier permeability (logBB), and central nervous system (CNS) permeability. Metabolism is predicted depending on the CYP models for substrate or inhibition. Excretion is predicted on the basis of the total clearance and the renal OCT2 substrate. Toxicity of the drugs is predicted on the basis of Ames toxicity, hERG inhibition, hepatotoxicity, and skin sensitization. These parameters were calculated for the four highest potent quinoline derivatives, **14**, **17**, **20**, and **23**, as well as for reference marketed antimicrobial agents. After evaluation of the ADMET properties (Table 5), we can propose that these derivatives have the advantage of better

intestinal absorption in humans over all the reference drugs (84.168–97.334), with zero in the case of amphotericin B and 13.46–43.034 in the case of ampicillin and gentamicin, respectively. This advantage may be attributed to the superior lipophilicity of the new ligands, which would make it easier to pass through the biological membranes.[34] Therefore, they may have a good bioavailability after the oral administration. The analysis of the CNS permeability revealed that the amide derivative **14** displayed the highest ability to penetrate the CNS (CNS permeability = −1.55), whereas the reference antimicrobials displayed lower abilities to penetrate (CNS permeability ≤ −3.16). Additionally, it was clear that in contrast to the three reference drugs, all the new compounds, except **20**, could inhibit the main cytochrome involved in drug metabolism, cytochrome P3A. This may also attribute to the higher lipophilicity of our newly synthesized quinolines. Excretion was evaluated in the terms of total clearance, a parameter that is associated with bioavailability and is taken into account while deciding dose timing intervals. Observed data demonstrated that the ester derivative **20** and gentamicin revealed the highest total clearance values (0.427 and 0.722, respectively), compared with other ligands, especially **17**, and amphotericin B, which showed the lowest total clearance value (0.139 and −1.495, respectively). Thus, **17** is expected to be excreted faster and consequently needs shorter dosing intervals. The last parameter studied in the ADMET profile of our newly synthesized quinolines is the toxicity. As shown in Table 5, ampicillin and all the new ligands, except **14**, share the disadvantage of hepatotoxicity. One critical disadvantage of the new quinolines is the probability of Ames toxicity, which means that the new ligands are expected to be mutagenic and hence may act as a carcinogen. Our designed compound **20** satisfactorily showed comparable tolerability (0.513) with that of ampicillin and gentamicin and better tolerability than that of amphotericin B (0.292). Finally, the oral acute toxic doses of the new compounds (LD_{50}) are also close to that of gentamicin and amphotericin B, which are higher than that of ampicillin.

3 | CONCLUSION

The present study reports the synthesis and in vitro antimicrobial evaluation of novel quinoline derivatives as potential DNA gyrase inhibitors. The preliminary antimicrobial activity was assessed against a panel of pathogenic microbes including two Gram-positive bacteria (*S. pneumoniae* and *B. subtilis*), two Gram-negative bacteria (*P. aeruginosa* and *E. coli*), and four fungal strains (*A. fumigatus*, *S. racemosum*, *G. candidum*, and *C. albicans*). The highest active compounds were subjected to further biological studies to determine their MICs against the selected pathogens as well as their in vitro activity against the *E. coli* DNA gyrase to realize whether their effect is mediated via inhibition of this enzyme. Four of the new derivatives (**14**, **17**, **20**, and **23**) displayed a relatively potent antimicrobial activity with MIC values ranging between 0.66 and 5.29 μg/ml. Among them, compound **14** exhibited a particularly potent broad-spectrum antimicrobial activity against the majority of the tested strains, with MIC values ranging from 0.66 to 3.98 μg/ml. A subsequent in vitro investigation against the bacterial DNA gyrase target enzyme revealed a significant potent inhibitory activity of compound **14** with an IC_{50} value of 3.39 μM. In addition, the structure–activity relationship of the synthesized compounds was discussed. Also, a molecular docking study of the most active compounds was carried out to predict the binding affinity toward the active site of DNA gyrase enzyme as a proposed target of their activity. Furthermore, ADMET profiles of the highest effective derivatives were examined to evaluate the potentials of the new compounds to be developed as good drug candidates. This study led to the identification of four novel quinoline derivatives with an interesting antimicrobial activity and DNA inhibitory potentials at relatively low micromolar concentrations.

4 | EXPERIMENTAL

4.1 | Chemistry

4.1.1 | General

Melting points were measured using an Electrothermal (Stuart SMP30) apparatus and were uncorrected. Infrared spectra were recorded on a Pye Unicam SP1000 IR spectrophotometer at the Pharmaceutical Analytical Unit, Faculty of Pharmacy, Al-Azhar University. ^{1}H NMR and ^{13}C NMR spectra were recorded in dimethyl sulfoxide (DMSO)-d_6 at 300 and 100 MHz, respectively, on a Varian Mercury VXR-300 NMR spectrometer at NMR Lab, Faculty of Science, Cairo University. Chemical shifts were related to that of the solvent, and tetramethylsilane was used as an internal standard. Coupling constant and chemical shift values are mentioned in Hz and ppm, respectively. Mass spectra and elemental analyses were carried out at the Regional Center for Mycology and Biotechnology, Al-Azhar University, Cairo, Egypt. The progress of reactions was monitored with Merck silica gel IB2-F plates (0.25 mm thickness) and was visualized under a UV lamp using different solvent systems as mobile phases. Reagents and starting *p*-toluidine, phosphorus oxychloride, chloroacetyl chloride, chloropropionyl chloride, and aniline derivatives were purchased from Sigma-Aldrich chemical company and were used as received. 2-Chloro-*N*-arylacetamides and 3-chloro-*N*-arylpropanamides were prepared following the reported procedures.[21,35] Compound **11** was synthesized according to directions of previously reported procedures.[8,13]

The InChI codes of the investigated compounds, together with some biological activity data, are provided as Supporting Information.

4.1.2 | General procedures for the synthesis of 2-[(3-cyano-6-methylquinolin-2-yl)thio]-*N*-arylacetamides and 3-[(3-cyano-6-methylquinolin-2-yl)thio]-*N*-(*m*-tolyl)propanamides 12–19

As displayed in Scheme 2, 2-mercapto-6-methylquinoline-3-carbonitrile (0.20 g, 0.001 mol) was suspended in a solution of potassium carbonate (0.025 mol) in DMF (30 ml). An appropriate quantity of

2-chloro-*N*-arylacetamide or 3-chloro-*N*-arylpropanamide derivative[36–38] (0.011 mol) was added, and the reaction mixture was heated to 120°C for 7 hr with continuous stirring. After the reaction was completed (monitored by TLC), the mixture was allowed to stand overnight. Later, after adding distilled cold water (100 ml), the obtained solid products were collected through filtration, washed with three repetitive portions of cold water (100 ml each) to remove the side salt product triethylammonium chloride, dried, crystallized from ethanol, and finally purified by using the column chromatography technique using hexane ethyl acetate as an eluent to afford the pure amide derivatives (**12**–**29**) in reasonable yields.

N-*(4-Chlorophenyl)-2-[(3-cyano-6-methylquinolin-2-yl)thio]-acetamide (**12**)*

Yellowish white solid. Yield: 85%; m.p. 230°C. IR (KBr) cm^{-1}: 3,295 (NH), 3,051 (CH aromatic), 2,904 (CH aliphatic), 2,221 (C≡N), 1,689 (C═O). ^{1}H NMR (DMSO-d_6) δ ppm: 9.89 (s, 1H, NH, D_2O-exchangeable), 8.9 (s, 1H, quinoline-H4), 7.8 (d, 1H, J = 9.0 Hz, quinoline-H8), 7.5 (d, 1H, J = 9.0 Hz, quinoline-H7), 7.4 (d, 2H, J = 9.6 Hz, phenyl-H2, H6), 7.1 (d, 2H, J = 9.6 Hz, phenyl-H3, H5), 7.3 (s, 1H, quinoline-H5), 4.37 (s, 2H, S–CH_2), 2.49 (s, 3H, CH_3). ^{13}C NMR (DMSO-d_6, 100 MHz) δ (ppm): 18.11 (CH_3), 34.75 (S–CH_2), 104.56, 115.90, 126.53, 127.32, 127.53, 127.62, 135.04, 135.30, 135.67, 135.83, 143.51, 146.45, and 156.17 (aromatic carbons), 123.84 (C≡N), and 165.57 (C═O). MS (*m*/*z*): 369 ($C_{19}H_{14}ClN_3OS$, 1.53%, M +2), 367 ($C_{19}H_{14}ClN_3OS$, 4.17%, M^+), 241 ($C_{13}H_9N_2OS$, 100%), 213 ($C_{12}H_9N_2S$, 46.37%), 199 ($C_{11}H_7N_2S$, 1.52%), 167 ($C_{11}H_7N_2$, 15.69%), 90 (C_7H_6, 4%). Anal. calc. for $C_{19}H_{14}ClN_3OS$ (M.W. = 367): C, 62.04; H, 3.42; N, 11.42%; found: C, 62.16; H, 3.91; N, 11.53%.

2-[(3-Cyano-6-methylquinolin-2-yl)thio]-N-*(*m*-tolyl)acetamide (**13**)*

Yellowish solid. Yield: 85%; m.p. 210°C. IR (KBr) cm^{-1}: 3,254 (NH), 3,043 (CH aromatic), 2,976 (CH aliphatic), 2,223 (C≡N), 1,662 (C═O). ^{1}H NMR (DMSO-d_6) δ ppm: 10.30 (s, 1H, NH, D_2O-exchangeable), 8.81 (s, 1H, quinoline-H4), 7.82 (d, 1H, J = 9.0 Hz, quinoline-H8), 7.77 (d, 1H, J = 9.0 Hz, quinoline-H7), 7.53 (s, 1H, phenyl-H2), 7.44 (s, 1H, quinoline-H5), 7.32 (d, 1H, J = 7.8 Hz, phenyl-H6), 7.25 (t, 1H, J = 10.80 Hz, phenyl-H5), 6.80 (d, 1H, J = 6 Hz, phenyl-H4), 4.29 (s, 2H, S–CH_2), 2.26 (s, 3H, quinoline-CH_3), 2.26 (s, 3H, phenyl-CH_3). ^{13}C NMR (DMSO-d_6, 100 MHz) δ (ppm): 18.09 (CH_3), 19.17 (CH_3), 34.73 (S–CH_2), 104.54, 115.90, 126.51, 127.30, 127.54, 127.60, 135.05, 135.32, 135.69, 135.85, 143.51, 146.43, and 156.16 (aromatic carbons), 123.86 (C≡N), and 165.55 (C═O). MS (*m*/*z*): 347 ($C_{20}H_{17}N_3OS$, 9.6%, M^+), 241 ($C_{13}H_9N_2OS$, 100%), 213 ($C_{12}H_9N_2S$, 70.6%), 199 ($C_{11}H_7N_2S$, 2.5%), 167 ($C_{11}H_7N_2$, 28.1%), 90 (C_7H_6, 2.8%). Anal. calc. for $C_{20}H_{17}N_3OS$ (M.W. = 347): C, 69.14; H, 4.93; N, 12.09%; found: C, 69.36; H, 5.1; N, 12.26%.

2-[(3-Cyano-6-methylquinolin-2-yl)thio]-N-*(2,6-dichlorophenyl)-acetamide (**14**)*

White solid. Yield: 85%; m.p. 250°C. IR (KBr) cm^{-1}: 3,241 (NH), 3,022 (CH aromatic), 2,957 (CH aliphatic), 2,226 (C≡N), 1,673 (C═O). ^{1}H NMR (DMSO-d_6) δ ppm: 10.20 (s, 1H, NH, D_2O-exchangeable), 8.9 (s, 1H, quinoline-H4), 7.90 (d, 1H, J = 9 Hz, quinoline-H8), 7.72 (d, 2H, J = 6 Hz, phenyl-H3, H5), 7.43 (d, 1H, J = 9.0 Hz, quinoline-H7), 7.31 (t, 1H, J = 6 Hz, phenyl-H4) 7.50 (s, 1H, quinoline-H5), 4.31 (s, 2H, S–CH_2), 2.5 (s, 3H, CH_3). ^{13}C NMR (DMSO-d_6, 100 MHz) δ (ppm): 18.06 (CH_3), 34.70 (S–CH_2), 104.51, 115.85, 126.48, 127.27, 127.48, 127.57, 134.99, 135.25, 135.62, 135.78, 143.46, 146.41, and 156.12 (aromatic carbons), 123.82 (C≡N), and 165.52 (C═O). MS (*m*/*z*): 403 ($C_{19}H_{13}Cl_2N_3OS$, 2.1%, M+2), 401 ($C_{19}H_{13}Cl_2N_3OS$, 3.8%, M^+), 241 ($C_{13}H_9N_2OS$, 100%), 199 ($C_{11}H_7N_2S$, 13.9%), 167 ($C_{11}H_7N_2$, 34.7%). Anal. calc. for $C_{19}H_{13}Cl_2N_3O_2S$ (M.W. = 401): C, 56.73; H, 3.26; N, 10.45%; found: C, 56.91; H, 3.39; N, 10.66%.

2-[(3-Cyano-6-methylquinolin-2-yl)thio]-N-*(2,6-dimethylphenyl)-acetamide (**15**)*

White solid. Yield: 70%; m.p. 270°C. IR (KBr) cm^{-1}: 3,249 (NH), 3,028 (CH aromatic), 2,984 (CH aliphatic), 2,222 (C≡N), 1,660 (C═O). ^{1}H NMR (DMSO-d_6) δ ppm: 9.6 (s, 1H, NH, D_2O-exchangeable), 8.9 (s, 1H, quinoline-H4), 7.91 (d, 1H, J = 9 Hz, quinoline-H8), 7.83 (d, 2H, J = 6 Hz, phenyl-H3, H5), 7.72 (d, 1H, J = 9.0 Hz, quinoline-H7), 7.02 (t, 1H, J = 6 Hz, phenyl-H4), 7.54 (s, 1H, quinoline-H5), 4.33 (s, 2H, S–CH_2), 2.50 (s, 3H, quinoline-CH_3), 2.08 (s, 6H, phenyl-2CH_3). ^{13}C NMR (DMSO-d_6, 100 MHz) δ (ppm): 18.06, 20.26, 33.71 (aliphatic carbons), 104.52, 115.86, 126.49, 127.28, 127.49, 127.58, 135.00, 135.26, 135.63, 136.78, 143.47, 146.42, and 156.13 (aromatic carbon atoms), 123.83 (C≡N), and 165.53 (C═O). MS (*m*/*z*), 361 ($C_{21}H_{19}N_3OS$, .85%, M^+), 241 ($C_{13}H_9N_2OS$, 90.6%), 213 ($C_{12}H_9N_2S$, 100%), 199 ($C_{11}H_7N_2S$, 18.3%). Anal. calc. for $C_{21}H_{19}N_3OS$ (M.W. = 361): C, 69.78; H, 5.3; N, 11.63%; found: C, 69.91; H, 5.39; N, 11.76%.

2-[(3-Cyano-6-methylquinolin-2-yl)thio]-N-*(4-methoxyphenyl)-acetamide (**16**)*

Greyish white solid. Yield: 85%; m.p. 225°C. IR (KBr) cm^{-1}: 3,257 (NH), 3,049 (CH aromatic), 2,922 (CH aliphatic), 2,223 (C≡N), 1,662 (C═O). ^{1}H NMR (DMSO-d_6) δ ppm: 10.26 (s, 1H, NH, D_2O-exchangeable), 8.82 (s, 1H, quinoline-H4), 7.85 (d, 1H, J = 9.0 Hz, quinoline-H8), 7.7 (d, 1H, J = 9.0 Hz, quinoline-H7), 7.51 (d, 2H, J = 9.6 Hz, phenyl-H2, H6), 6.82 (d, 2H, J = 9.6 Hz, phenyl-H3, H5), 7.43 (s, 1H, quinoline-H5), 4.24 (s, 2H, S–CH_2), 3.34 (s, 3H, phenyl-OCH_3), 2.40 (s, 3H, quinoline-CH_3). ^{13}C NMR (DMSO-d_6, 100 MHz) δ (ppm): 18.19 (CH_3), 34.83 (S–CH_2), 57.26 (OCH_3), 104.64, 115.98, 126.61, 127.40, 127.64, 127.70, 135.15, 135.42, 135.79, 135.95, 143.61, 146.53, and 156.26 (aromatic carbons), 123.88 (C≡N), and 165.65 (C═O). MS (*m*/*z*): 363 ($C_{20}H_{17}N_3O_2S$, 9.4%, M^+), 241 ($C_{13}H_9N_2OS$, 21.54%), 213 ($C_{12}H_9N_2S$, 14.9%), 123 (C_7H_9NO, 100%). Anal. calc. for $C_{20}H_{17}N_3O_2S$ (M.W. = 363): C, 66.10; H, 4.71; N, 1.56%; found: C, 66.19; H, 4.74; N, 11.61%.

2-[(3-Cyano-6-methylquinolin-2-yl)thio]-N-*(4-nitrophenyl)-acetamide (**17**)*

Yellowish white solid. Yield: 85%; m.p. 230°C. IR (KBr) cm^{-1}: 3,227 (NH), 3,043 (CH aromatic), 2,929 (CH aliphatic), 2,221 (C≡N), 1,675 (C═O). ^{1}H NMR (DMSO-d_6) δ ppm: 11.02 (s, 1H, NH, D_2O-exchangeable), 8.9 (s, 1H, quinoline-H4), 8.21 (d, 1H, J = 9.0 Hz,

quinoline-H8), 7.80 (d, 1H, *J* = 9.0 Hz, quinoline-H7), 7.71 (d, 2H, *J* = 9.6 Hz, phenyl-H2, H6), 7.13 (d, 2H, *J* = 9.6, phenyl-H3, H5), 7.36 (s, 1H, quinoline-H5), 4.37 (s, 2H, S–CH_2), 2.46 (s, 3H, CH_3). ^{13}C NMR (DMSO-d_6, 100 MHz) δ (ppm): 18.15 (CH_3), 34.79 (S–CH_2), 104.60, 115.95, 126.57, 127.36, 127.63, 127.68, 135.11, 135.38, 135.75, 135.98, 143.63, 146.47, and 156.21 (aromatic carbons), 123.85 (C≡N), and 165.62 (C═O). MS (*m/z*): 378 ($C_{19}H_{14}N_4O_3S$, 3.26%, M^+), 241 ($C_{13}H_9N_2OS$, 100%), 199 ($C_{11}H_7N_2S$, 2.86%), 167 ($C_{11}H_7N_2$, 27.8%). Anal. calc. for $C_{19}H_{14}N_4O_3S$ (M.W. = 378): C, 60.31; H, 3.73; N, 14.81%; found: C, 60.39; H, 3.75; N, 14.89%.

*2-[(3-Cyano-6-methylquinolin-2-yl)thio]-*N*-(2,4,6-tribromophenyl)-acetamide (**18**)*

Yellow white solid. Yield: 75%; m.p. 285°C. IR (KBr) cm^{-1}: 3,216 (NH), 3,045 (CH aromatic), 2,989 (CH aliphatic), 2,226 (C≡N), 1,663 (C═O), 636 (C–Br). ^{1}H NMR (DMSO-d_6) δ ppm: 10.27 (s, 1H, NH, D_2O-exchangeable), 8.92 (s, 1H, quinoline-H4), 7.98 (d, 1H, *J* = 9.0 Hz, quinoline-H8), 7.91 (s, 2H, phenyl-H3, H5), 7.75 (d, 1H, *J* = 9.0 Hz, quinoline-H7), 7.78 (s, 1H, quinoline-H5), 4.36 (s, 2H, S–CH_2), 2.36 (s, 3H, quinoline-CH_3). ^{13}C NMR (DMSO-d_6, 100 MHz) δ (ppm): 18.25 (CH_3), 34.87 (S–CH_2), 104.71, 116.06, 126.67, 127.46, 127.63, 127.78, 135.21, 135.47, 135.66, 136.09, 143.72, 146.56, and 156.30 (aromatic carbons), 123.87 (C≡N), and 165.71 (C═O). MS (*m/z*): 570 ($C_{19}H_{12}Br_3N_3OS$, 2.97%, M+2), 568 ($C_{19}H_{12}Br_3N_3OS$, 2.97%, M^+), 241 ($C_{13}H_9N_2OS$, 100%), 213 ($C_{12}H_9N_2S$, 44.4%). Anal. calc. for $C_{19}H_{12}Br_3N_3OS$ (M.W. = 570): C, 40.04; H, 2.12; N, 7.37%; found: C, 40.29; H, 2.33; N, 7.49%.

*3-[(3-Cyano-6-methylquinolin-2-yl)thio]-*N*-(m-tolyl)-propanamide (**19**)*

Pale yellow solid. Yield: 85%; m.p. 230°C. IR (KBr) cm^{-1}: 3,256 (NH), 3,021 (CH aromatic), 2,920 (CH aliphatic), 2,223 (C≡N), 1,647 (C═O). ^{1}H NMR (DMSO-d_6) δ ppm: 9.30 (s, 1H, NH, D_2O-exchangeable), 8.86 (s, 1H, quinoline-H4), 7.80 (d, 1H, *J* = 9.0 Hz, quinoline-H8), 7.73 (d, 1H, *J* = 9.0 Hz, quinoline-H7), 7.44 (s, 1H, phenyl-H2), 7.31 (s, 1H, quinoline-H5), 7.20 (d, 1H, *J* = 7.8 Hz, phenyl-H6), 7.1 (t, 1H, *J* = 15 Hz, phenyl-H5), 7.01 (d, 1H, *J* = 6 Hz, phenyl-H4), 3.68 (t, 2H, S–CH_2), 2.8 (t, 2H, CH_2–C═O), 2.49 (s, 3H, quinoline-CH_3), 2.19 (s, 3H, phenyl-CH_3). ^{13}C NMR (DMSO-d_6, 100 MHz) δ (ppm): 20.09 (CH_3), 19.17 (CH_3), 34.73 (S–CH_2), 32.73 (CH_2CO), 104.53, 115.90, 126.50, 127.30, 127.53, 127.61, 135.04, 135.33, 135.68, 135.85, 143.51, 146.42, and 156.14 (aromatic carbons), 123.84 (C≡N), and 165.56 (C═O). MS (*m/z*): 361 ($C_{21}H_{19}N_3OS$, 14.07%, M^+), 255 ($C_{14}H_{11}N_2OS$, 16.48%), 227 ($C_{13}H_{11}N_2S$, 80.46%), 200 ($C_{11}H_7N_2S$, 11.36%). Anal. calc. for $C_{21}H_{19}N_3OS$ (M.W. = 361): C, 69.78; H, 5.30; N, 11.63%; found: C, 69.96; H, 5.39; N, 11.76%.

4.1.3 | General procedures for the synthesis of alkyl 2-[(3-cyano-6-methylquinolin-2-yl)thio]acetate/propanoate 20–22

2-Mercapto-6-methylquinoline-3-carbonitrile (0.20 g, 0.001 mol) was suspended in a solution of potassium carbonate (0.025 mol) in DMF (30 ml). An appropriate quantity of α-chloroester derivative (0.011 mol) was added, and the reaction mixture was heated to 90°C for 7 hr with continuous stirring. After the reaction was completed (monitored by TLC), the mixture allowed to stand overnight. Later, after adding distilled cold water (100 ml), the obtained solid products were collected through filtration, washed with three repetitive portions of cold water (100 ml each) to remove the side salt product triethylammonium chloride, dried, crystallized from ethanol, and finally purified by using column chromatography technique using hexane ethyl acetate as an eluent to afford the pure amide derivatives (**12**–**29**) in reasonable yields.

*Methyl 2-[(3-cyano-6-methylquinolin-2-yl)thio]acetate (**20**)*

Yellow solid. Yield: 85%; m.p. 135°C. IR (KBr) cm^{-1}: 3,069 (CH aromatic), 2,953 (CH aliphatic), 2,222 (C≡N), 1,729 (C═O). ^{1}H NMR (DMSO-d_6) δ ppm: 9.12 (s, 1H, quinoline-H4), 7.93 (d, 1H, *J* = 9.0 Hz, quinoline-H8), 7.60 (d, 1H, *J* = 9.0 Hz, quinoline-H7), 7.54 (s, 1H, quinoline-H5), 3.82 (s, 2H, S–CH_2), 3.32 (s, 3H, CO_2CH_3), 2.50 (s, 3H, CH_3). ^{13}C NMR (DMSO-d_6, 100 MHz) δ (ppm): 20.09 (CH_3), 30.73 (S–CH_2), 51.17 (OCH_3), 104.53, 122.50, 126.30, 128.93, 134.61, 138.54, 140.97, 144.68, 159.85 (aromatic carbons), 121.80 (C≡N), and 169.56 (C═O). MS (*m/z*): 272 ($C_{14}H_{12}N_2O_2S$, 28.8%, M^+), 241 ($C_{13}H_9N_2OS$, 8.63%), 213 ($C_{12}H_9N_2S$, 100%). Anal. calc. for $C_{14}H_{12}N_2O_2S$ (M.W. = 272): C, 61.75; H, 4.44; N, 10.29%; found: C, 61.87; H, 4.49; N, 10.38%.

*Ethyl 2-[(3-cyano-6-methylquinolin-2-yl)thio]acetate (**21**)*

Yellow solid. Yield: 85%; m.p. 129°C. IR (KBr) cm^{-1}: 3,060 (CH aromatic), 2,980 (CH aliphatic), 2,222 (C≡N), 1,731 (C═O). ^{1}H NMR (DMSO-d_6) δ ppm: 9.12 (s, 1H, H4), 7.9 (d, 1H, *J* = 8.4 Hz, quinoline-H8), 7.6 (d, 1H, *J* = 9.0 Hz, quinoline-H7), 7.5 (s, 1H, H5), 4.3 (q, 2H, *J* = 21 Hz, OCH_2), 3.3 (s, 2H, S–CH_2), 2.49 (s, 3H, CH_3), 1.3 (t, 3H, *J* = 15 Hz, –CH_3). ^{13}C NMR (DMSO-d_6, 100 MHz) δ (ppm): 15.12 (CH_3), 20.09 (CH_3), 30.72 (S–CH_2), 58.17 (OCH_2), 104.52, 122.50, 126.28, 128.86, 134.59, 138.54, 140.95, 144.66, 159.84 (aromatic carbons), 121.81 (C≡N), and 169.58 (C═O). MS (*m/z*): 286 ($C_{15}H_{14}N_2O_2S$, 10.9%, M^+), 241 ($C_{13}H_9N_2OS$, 7.35%), 213 ($C_{12}H_9N_2S$, 100%). Anal. calc. for $C_{15}H_{14}N_2O_2S$ (M.W. = 286): C, 62.92; H, 4.93; N, 9.78%; found: C, 62.45; H, 4.56; N, 9.78%.

*Ethyl 2-[(3-cyano-6-methylquinolin-2-yl)thio]propanoate (**22**)*

Yellow solid. Yield: 85%; m.p. 160°C. IR (KBr) cm^{-1}: 3,052 (CH aromatic), 2,977 (CH aliphatic), 2,221 (C≡N), 1,729 (C═O). ^{1}H NMR (DMSO-d_6) δ ppm: 8.89 (s, 1H, quinoline-H4), 7.90 (d, 1H, *J* = 9.0 Hz, quinoline-H8), 7.61 (d, 1H, *J* = 9.0 Hz, quinoline-H7), 7.54 (s, 1H, quinoline-H5), 4.61 (q, 1H, *J* = 12 Hz, S–CH), 4.12 (q, 2H, *J* = 10.8 Hz, OCH_2), 2.36 (s, 3H, CH_3), 1.62 (d, 3H, *J* = 12 Hz, S–CH–CH_3), 1.15 (t, 3H, *J* = 15 Hz, CH_2–CH_3). ^{13}C NMR (DMSO-d_6, 100 MHz) δ (ppm): 14.09 (CH_3), 17.23 (CH_3), 24.89 (CH_3), 32.34 (S–CH), 60.04, (OCH_2), 104.18, 115.67, 127.10, 131.23, 135.32, 143.50, 146.24, 147.11, 158.90 (aromatic carbon atoms), 123.74 (C≡N), and 168.48 (C═O). MS (*m/z*): 300 ($C_{16}H_{16}N_2O_2S$, 7.17%, M^+), 255 ($C_{14}H_{11}N_2OS$, 4.59%), 227 ($C_{13}H_{11}N_2S$, 100%). Anal. calc. for $C_{16}H_{16}N_2O_2S$ (M.W. = 300): C, 63.98; H, 5.37; N, 9.33%; found: C, 63.92; H, 5.46; N, 9.41%.

4.1.4 | Synthesis of 2-[(3-cyano-6-methylquinolin-2-yl)thio]acetohydrazide (23)

A mixture of **21** (10 mmol) and hydrazine hydrate 80% (0.5 ml, 10 mmol) in absolute ethanol (50 ml) was refluxed for 4 hr. The reaction mixture was cooled in an ice bath and diluted with water (50 ml). The produced precipitate was filtered off and recrystallized from ethanol as transparent plates. Yield: 90%; m.p. over 290°C. IR (KBr) cm^{-1}: 3,418 (NH_2), 3,125 (NH), 3,046 (CH aromatic), 2,983 (CH aliphatic), 2,224 (C≡N), 1,666 (C═O). ^{1}H NMR (DMSO-d_6) δ ppm: 8.86 (s, 1H, NH, D_2O-exchangeable), 9.38 (s, 1H, quinoline-H4), 7.82 (d, 1H, J = 9.0 Hz, quinoline-H8), 7.73 (d, 1H, J = 9.0 Hz, quinoline-H7), 7.45 (s, 1H, quinoline-H5), 4.30 (s, 2H, NH_2), 4.07 (s, 2H, S–CH_2), 2.55 (s, 3H, quinoline-CH_3). ^{13}C NMR (DMSO-d_6, 100 MHz) δ (ppm): 14.09 (CH_3), 39.89 (S–CH_2), 104.18, 115.67, 127.10, 131.23, 135.32, 143.50, 146.24, 147.11, 158.90 (aromatic carbon atoms), 123.74 (C≡N), and 168.48 (C═O). MS (*m/z*): 272 ($C_{13}H_{12}N_4OS$, 4.2%, M^+), 240 ($C_{13}H_9N_2OS$, 100.11%), 213 ($C_{12}H_9N_2S$, 40.13%), 200 ($C_{11}H_8N_2S$, 25.3%). Anal. calc. for $C_{13}H_{12}N_4OS$ (M.W. = 272): C, 57.34; H, 4.44; N, 20.57%; found: C, 57.41; H, 4.41; N, 20.61%.

4.2 | In vitro antimicrobial evaluation

The agar diffusion method[39,40] was used for the determination of antibacterial and antifungal activity. The microorganisms were spread uniformly using sterile cotton swabs on a sterile malt extract agar Petri dish for fungi and nutrient agar for bacteria. A volume of 100 cm^3 of each sample was added to each well (10-mm-diameter holes were cut in the agar gel, 20 mm apart from one another). The systems were incubated for 24–48 hr at 37°C for bacteria and at 28°C for fungi. After the incubation period, microorganism growth was observed, and the IZs of the bacterial and fungal growth were measured in millimeters. Tests were performed in triplicate.

4.2.1 | Determination of the IZs

Here, 75 μl from a solution of each test compound (1 mg/ml in DMF) was put in a 6-mm-diameter well in an agar plate seeded with the appropriate test pathogen in triplicates. Ampicillin (5.0 μg/disc), gentamicin (5.0 μg/disc), and amphotericin B (100.0 μg/disc) were used as standards for Gram-positive, Gram-negative antibacterial, and antifungal agents, respectively. DMF as a negative control showed no IZ. Plates were incubated at 37°C for 24 hr. Samples that showed IZ ≥ 19 mm were selected for further biological evaluation to measure their MIC.[39]

4.2.2 | Determination of the MIC

The MICs of derivatives that showed IZ ≥ 19 mm and reference drugs were determined as described by the *Performance Standards for Antimicrobial Susceptibility Testing*: 11th Informational Supplement; National Committee for Clinical Laboratory Standards.[29] The MIC values were defined as the lowest concentration of each compound that results in an inhibition of the visible growth of bacteria after incubation at 37°C for 18–24 hr, as detected by unaided eye.

4.2.3 | DNA gyrase supercoiling inhibition assay

IC_{50} values were determined using high-throughput assay[30] on black streptavidin-coated 96-well microtiter plates. Novobiocin was used as a positive control. IC_{50} values were calculated using the GraphPad Prism software and they represent the concentration of a compound where the residual enzyme activity is 50%, as observed in three independent tests. Results are given as their average values in μM (see Supporting Information Data).

4.3 | Docking studies

Molecular docking experiments were conducted by MOE builder within the MOE software suite (MOE2014, https://www.chemcomp.com/Products.htm) to evaluate the binding free energy and to discover the binding mode toward DNA gyrase enzyme (PDB: 4DUH, resolution: 2.70 Å, https://www.rcsb.org/structure/4DUH), which is considered as a target for docking simulation.[31] The crystal structure of the protein was first prepared by removing water molecules and retaining the essential chain and the internal co-crystallized ligand (RLI). Next, hydrogen atoms were added to the structure, the energy was minimized, and the binding pocket of the protein was defined. The 3D structures of new quinolines were sketched using ChemDraw3D 15.0, their energies were minimized, and finally saved in molfile format. Molecular docking of the four most active quinoline derivatives was performed by the default protocol against the target receptor. In each case, 20 docked poses were generated using genetic algorithm searches, and Affinity dG and London dG were used for Scoring 1 and Scoring 2, respectively. The London dG scoring function predicts the free energy of binding of the ligand from a given pose. The functional form is a sum of terms:

$$\Delta G = C + E_{\text{flex}} + \sum_{\text{h-bond}} C_{\text{HB}} F_{\text{HB}} + \sum_{\text{m-lig}} C_{\text{M}} F_{\text{M}} + \sum_{\text{atom i}} \Delta D_{\text{i}},$$

where C is the average gain or loss of rotational and translational entropy; E_{flex} represents the energy upon loss of flexibility of the ligand; C_{HB} and F_{HB} are the energy of an ideal hydrogen bond and the geometric imperfections of hydrogen bonds, respectively; C_{M} and F_{M} represent the energy of an ideal metal ligation and the measure of geometric imperfections of metal ligations, respectively; and D_{i} is the desolvation energy of an atom *i*.

CONFLICTS OF INTERESTS

The authors declare that there are no conflicts of interests.

ORCID

Khaled El-Adl http://orcid.org/0000-0002-8922-9770

Hany E. A. Ahmed http://orcid.org/0000-0001-8898-8452

Hamada S. Abulkhair http://orcid.org/0000-0001-6479-4573

REFERENCES

[1] J. Hyde, C. Gorham, D. E. Brackney, B. Steven, *PLOS One* **2019**, *14*, e0218907. https://doi.org/10.1371/journal.pone.0218907

[2] Antimicrobial resistance, https://www.who.int/news-room/fact-sheets/detail/antimicrobial-resistance (accessed: July 2020).

[3] P. Loomba, J. Taneja, B. Mishra, *J. Global Infect. Dis.* **2010**, *2*, 275. https://doi.org/10.4103/0974-777X.68535

[4] A. K. McClendon, N. Osheroff, *Mutat. Res., Fundam. Mol. Mech. Mutagen.* **2007**, *623*, 83. https://doi.org/10.1016/j.mrfmmm.2007.06.009

[5] D. C. Hooper, G. A. Jacoby, *Cold Spring Harbor Perspect. Med.* **2016**, *6*, a025320. https://doi.org/10.1101/cshperspect.a025320

[6] T. D. M. Pham, Z. M. Ziora, M. A. T. Blaskovich, *MedChemComm* **2019**, *10*, 1719. https://doi.org/10.1039/C9MD00120D

[7] A. M. Omar, M. Alswah, H. E. A. Ahmed, A. H. Bayoumi, K. M. El-Gamal, A. El-Morsy, A. Ghiaty, T. H. Afifi, F. F. Sherbiny, A. S. Mohammed, B. A. Mansour, *Bioorg. Chem.* **2020**, *96*, 103656. https://doi.org/10.1016/j.bioorg.2020.103656

[8] M. F. El Shehry, M. M. Ghorab, S. Y. Abbas, E. A. Fayed, S. A. Shedid, Y. A. Ammar, *Eur. J. Med. Chem.* **2018**, *143*, 1463. https://doi.org/10.1016/j.ejmech.2017.10.046

[9] J. W. Bennett, M. Klich, *Clin. Microbiol. Rev.* **2003**, *16*, 497. https://doi.org/10.1128/CMR.16.3.497-516.2003

[10] N. C. Desai, B. Y. Patel, B. P. Dave, *Med. Chem. Res.* **2017**, *26*, 109. https://doi.org/10.1007/s00044-016-1732-6

[11] M.-Z. Zhang, C.-Y. Jia, Y.-C. Gu, N. Mulholland, S. Turner, D. Beattie, W.-H. Zhang, G.-F. Yang, J. Clough, *Eur. J. Med. Chem.* **2017**, *126*, 669. https://doi.org/10.1016/j.ejmech.2016.12.001

[12] M. Hagrs, A. H. Bayoumi, K. M. El-Gamal, A. S. Mayhoub, H. S. Abulkhair, *Beni-Suef Univ. J. Basic Appl. Sci.* **2015**, *4*, 338. https://doi.org/10.1016/j.bjbas.2015.09.001

[13] K. M. El-Gamal, M. S. Hagrs, H. S. Abulkhair, *Bull. Fac. Pharm. (Cairo Univ.)* **2016**, *54*, 263. https://doi.org/10.1016/j.bfopcu.2016.08.002

[14] P. Nickel, E. Fink, *Arch. Pharm.* **1972**, *305*, 442. https://doi.org/10.1002/ardp.19723050607

[15] S. Bawa, S. Kumar, S. Drabu, R. Kumar, *J. Pharm. BioAllied Sci.* **2010**, *2*, 64. https://doi.org/10.4103/0975-7406.67002

[16] M. H. Hannoun, M. Hagras, A. Kotb, A.-A. M. M. El-Attar, H. S. Abulkhair, *Bioorg. Chem.* **2020**, *94*, 103364. https://doi.org/10.1016/J.BIOORG.2019.103364

[17] I. Eid, M. M. Elsebaei, H. Mohammad, M. Hagras, C. E. Peters, Y. A. Hegazy, B. Cooper, J. Pogliano, K. Pogliano, H. S. Abulkhair, M. N. Seleem, A. S. Mayhoub, *Eur. J. Med. Chem.* **2017**, *139*, 665. https://doi.org/10.1016/j.ejmech.2017.08.039

[18] M. P. Reddy, G. S. K. Rao, *J. Org. Chem.* **1981**, *46*, 5371. https://doi.org/10.1021/jo00339a023

[19] A. Bayoumi, A. Ghiaty, A. El-Morsy, H. Abul-Khair, M. H. Hassan, S. Elmeligie, *Bull. Fac. Pharm. (Cairo Univ.)* **2012**, *50*, 141. https://doi.org/10.1016/j.bfopcu.2012.05.002

[20] A. Turky, F. F. Sherbiny, A. Bayoumi, H. E. A. Ahmed, H. S. Abulkhair, *Arch. Pharm.* **2020**, e2000170. https://doi.org/10.1002/ardp.202000170

[21] A. Turky, A. H. Bayoumi, F. F. Sherbiny, K. El-Adl, H. S. Abulkhair, *Mol. Divers.* **2020**, https://doi.org/10.1007/s11030-020-10131-0

[22] K. El-Adl, A.-G A. El-Helby, H. Sakr, R. R. Ayyad, H. A. Mahdy, M. Nasser, H. S. Abulkhair, S. S. A. El-Hddad, *Arch. Pharm.* **2020**, e202000279.

[23] A. A. El-Helby, H. Sakr, I. H. Eissa, H. Abulkhair, A. A. Al-Karmalawy, K. El-Adl, *Arch. Pharm.* **2019**, *352*, 1900113. https://doi.org/10.1002/ardp.201900113

[24] S. Ihmaid, H. E. A. Ahmed, A. Al-Sheikh Ali, Y. E. Sherif, H. M. Tarazi, S. M. Riyadh, M. F. Zayed, H. S. Abulkhair, H. S. Rateb, *Bioorg. Chem.* **2017**, *72*, 234. https://doi.org/10.1016/j.bioorg.2017.04.014

[25] H. Abul-Khair, S. Elmeligie, A. Bayoumi, A. Ghiaty, A. El-Morsy, M. H. Hassan, *J. Heterocycl. Chem.* **2013**, *50*, 1202. https://doi.org/10.1002/jhet.714

[26] A. M. El-Morsy, M. S. El-Sayed, H. S. Abulkhair, *Open J. Med. Chem.* **2007**, *7*, 1.

[27] M. Balouiri, M. Sadiki, S. K. Ibnsouda, *J. Pharm. Anal.* **2015**, *6*, 71. https://doi.org/10.1016/j.jpha.2015.11.005

[28] B. Bonev, J. Hooper, J. Parisot, *J. Antimicrob. Chemother.* **2008**, *61*, 1295. https://doi.org/10.1093/jac/dkn090

[29] J. A. Kiehlbauch, G. E. Hannett, M. Salfinger, W. Archinal, C. Monserrat, C. Carlyn, *J. Clin. Microbiol.* **2000**, *38*, 3341. https://doi.org/10.1128/JCM.38.9.3341-3348.2000

[30] A. Maxwell, N. P. Burton, N. O'Hagan, *Nucleic Acids Res.* **2006**, *34*, e104. https://doi.org/10.1093/nar/gkl504

[31] M. Brvar, A. Perdih, M. Renko, G. Anderluh, D. Turk, T. Solmajer, *J. Med. Chem.* **2012**, *55*, 6413. https://doi.org/10.1021/jm300395d

[32] C. A. Lipinski, F. Lombardo, B. W. Dominy, P. J. Feeney, *Adv. Drug Deliv. Rev.* **1997**, *23*, 3. https://doi.org/10.1016/S0169-409X(96)00423-1

[33] D. E. V. Pires, T. L. Blundell, D. B. Ascher, *J. Med. Chem.* **2015**, *58*, 4066. https://doi.org/10.1021/acs.jmedchem.5b00104

[34] A. Beig, R. Agbaria, A. Dahan, *PLOS One* **2013**, *8*, e68237. https://doi.org/10.1371/journal.pone.0068237

[35] A. A. El-Helby, R. R. A. Ayyad, M. F. Zayed, H. S. Abulkhair, H. Elkady, K. El-Adl, *Arch. Pharm.* **2019**, *352*, 1800387. https://doi.org/10.1002/ardp.201800387

[36] H. S. Abulkhair, A. Turky, A. Ghiaty, H. E. A. Ahmed, A. H. Bayoumi, *Bioorg. Chem.* **2020**, *100*, 103899. https://doi.org/10.1016/j.bioorg.2020.103899

[37] A. M. Omar, S. Ihmaid, E. S. E. Habib, S. S. Althagfan, S. Ahmed, H. S. Abulkhair, H. E. A. Ahmed, *Bioorg. Chem.* **2020**, *99*, 103781. https://doi.org/10.1016/j.bioorg.2020.103781

[38] A. Turky, A. H. Bayoumi, A. Ghiaty, A. S. El-Azab, A. A.-M. Abdel-Aziz, H. S. Abulkhair, *Bioorg. Chem.* **2020**, *101*, 104019. https://doi.org/10.1016/j.bioorg.2020.104019

[39] M. Balouiri, M. Sadiki, S. K. Ibnsouda, *J. Pharm. Anal.* **2016**, *6*, 71. https://doi.org/10.1016/j.jpha.2015.11.005

[40] L. Jiang, F. Wang, F. Han, W. Prinyawiwatkul, H. K. No, B. Ge, *J. Appl. Microbiol.* **2013**, *114*, 956. https://doi.org/10.1111/jam.12111

SUPPORTING INFORMATION

Additional supporting information may be found online in the Supporting Information section.

How to cite this article: El-Shershaby MH, El-Gamal KM, Bayoumi AH, El-Adl K, Ahmed HEA, Abulkhair HS. Synthesis, antimicrobial evaluation, DNA gyrase inhibition, and in silico pharmacokinetic studies of novel quinoline derivatives. *Arch Pharm.* 2020;e2000277. https://doi.org/10.1002/ardp.202000277